Direct Dynamics Studies on Hydrogen Abstraction Reactions of CH_3CHFCH_3 and $CH_3CH_2CH_2F$ with OH Radicals

Ying Wang, Jing-yao Liu,* Lei Yang, Xiao-lei Zhao, Yue-meng Ji, and Ze-sheng Li*

Institute of Theoretical Chemistry, State Key Laboratory of Theoetical and Computational Chemistry, Jilin University, Changchun 130023, People's Republic of China

Received: January 19, 2007; In Final Form: May 13, 2007

The hydrogen abstraction reactions of CH_3CHFCH_3 and $CH_3CH_2CH_2F$ with the OH radicals have been studied theoretically by a dual-level direct dynamics method. The geometries and frequencies of all the stationary points are optimized by means of the DFT calculation. There are complexes at the reactant side or exit route, indicating these reactions may proceed via indirect mechanisms. To improve the reaction enthalpy and potential barrier of each reaction channel, the single point energy calculation is performed by the MC-QCISD/3 method. The rate constants are evaluated by canonical variational transition state theory (CVT) with the small-curvature tunneling correction method (SCT) over a wide temperature range 200−2000 K. The canculated CVT/SCT rate constants are consistent with available experimental data. The results show that both the variation effect and the SCT contribution play an important role in the calculation of the rate constants. For reactions CH_3CHFCH_3 and $CH_3CH_2CH_2F$ with OH radicals, the channels of H-abstraction from −CHF− and $-CH_2-$ groups are the major reaction channels, respectively, at lower temperature. Furthermore, to further reveal the thermodynamics properties, the enthalpies of formation of reactants CH_3CHFCH_3, $CH_3CH_2CH_2F$, and the product radicals CH_3CFCH_3, CH_3CHFCH_2, CH_3CH_2CHF, CH_3CHCH_2F, and $CH_2CH_2CH_2F$ are studied using isodesmic reactions.

Introduction

Concerning the adverse impact of chlorofluorocarbons (CFCs) on stratospheric ozone[1−3] and global warming,[4−8] an international effort has been made to replace CFCs with environmentally acceptable alternatives. Hydrofluorocarbons (HFCs) are one class of CFC replacements used in refrigeration and foam blowing and cleaning applications. They contain neither Cl nor Br and, thus, should pose no threat to the stratospheric ozone layer,[9] though they may contribute to the greenhouse effect because they contain numerous C−F bonds. As these HFC molecules have at least one C−H bond, they are therefore susceptible to attack by OH in the atmosphere. To estimate the atmospheric lifetimes of such species, accurate data for the rate constants and their temperature dependences of the reaction with OH radicals are needed. In this work, we focus on theoretical investigation on the kinetics of the reactions 2-fluoropropane (HFC-281ea) and 1-fluoropropane with hydroxyl radicals. There are two kinds of experimental techniques,[10] i.e., relative rate experiments using infrared spectroscopy and gas chromatography (GC), to measure the rate constants for the reaction OH + CH_3CHFCH_3. Results from the two measurement techniques are in good agreement. Note that the GC data are preferable due to the lower random error. Based on the GC experiments, the rate constant expression over the temperature range 288−394 K is $k = 3.06 \times 10^{-12} \exp(-503/T)$ cm^3 molecule^{-1} s^{-1}, with the value 5.7×10^{-13} cm^3 molecule^{-1} s^{-1} at 298 K. In ref 10, DeMore et al. also used a empirical rule[11] to predict the rate constant and its temperature dependence for reaction CH_3CHFCH_3 + OH. According to this method, each reactive site is considered to be a methane derivative, and the reactivity of the C−H bonds at that site is determined by the attached groups that have replaced the H-atoms in methane. The total rate constant is obtained as the sum of the contributions from each C−H bond present in the molecule. The predicted Arrhenius parameter over the temperature range 275−425 K is $k = 3.6 \times 10^{-12} \exp(-632/T)$ cm^3 molecule^{-1} s^{-1} and the rate constant at 298 K is $k(298\ \text{K}) = 4.3 \times 10^{-13}$ cm^3 molecule^{-1} s^{-1}, which are in good agreement with the GC experimental ones. However, for the reaction 1-fluoropropane with OH radicals, no experimental data except empirical prediction by DeMore et al. are reported. The estimated Arrhenius parameter over the temperature range 275−425 K is $k = 3.06 \times 10^{-12} \exp(-818/T)$ cm^3 molecule^{-1} s^{-1}. To the best of our knowledge, no other theoretical work has been performed for both reactions. The aim of present study is to perform a theoretical investigation for the title reactions to provide further information of the reaction mechanisms as well as the temperature dependence of the rate constants over a wide temperature range.

For the molecule CH_3CHFCH_3, the hydrogen atom can be abstracted from −CHF− (denoted as channel 1a) and $-CH_3$ (denoted as channel 1b) positions, and as a result of the asymmetry of CH_3CHFCH_3, the three hydrogen atoms lying at the $-CH_3$ position are not equivalent; then three distinct channels are found for channel 1b (denoted as channel 1b-α, 1b-β, and 1b-γ), i.e.,

$$CH_3CHFCH_3 + OH \rightarrow CH_3CFCH_3 + H_2O \quad \text{(R1a)}$$

$$\rightarrow CH_3CHFCH_2 + H_2O \quad \text{(R1b-α, R1b-}\beta\text{, R1b-}\gamma\text{)}$$

Note that, strictly speaking, because CH_3CHFCH_3 has C_1 symmetry, both CH_3 groups are not equivalent, and channels R1b-α, R1b-β, and R1b-γ should be calculated separately for both CH_3 groups. However, due to the similar structure of the transition states, here the same contribution of each group to rate constants is assumed. For the reactant $CH_3CH_2CH_2F$, there

* Corresponding authors. Fax: +86-431-88498026. E-mail: ljy121@mail.jlu.edu.cn, zeshengli@mail.jlu.edu.cn.

10.1021/jp0704665 CCC: $37.00
Published on Web 07/26/2007

are two stable conformers, SC_1 and SC_2. Based on calculations, SC_1 is only stabler than SC_2 by about 0.24 kcal/mol at the MC-QCISD/3//B3LYP level, so it is likely that these two conforms have similar stability and will both contribute to the overall rate constant. In SC_1 structure each hydrogen atom is not equivalent, and as a result, seven distinguished channels are found according to the different position of these seven H-atoms. These channels are defined as follows:

$$\begin{aligned} CH_3CH_2CH_2F\ (SC_1) + OH &\rightarrow CH_3CH_2CHF\ (P_{2a1}) + H_2O \\ &\qquad (R2a1\text{-}\alpha,\ R2a1\text{-}\beta) \\ &\rightarrow CH_2CH_2CH_2F\ (P_{2b1}) + H_2O \\ &\qquad (R2b1\text{-}\alpha,\ R2b1\text{-}\beta,\ R2b1\text{-}\gamma) \\ &\rightarrow CH_3CHCH_2F\ (P_{2c1}) + H_2O \\ &\qquad (R2c1\text{-}\alpha,\ R2c1\text{-}\beta) \end{aligned}$$

As for SC_2 with the C_s symmetry, the hydrogen atoms in the $-CH_2F$ and $-CH_2-$ groups are equivalent, with the corresponding reaction channels R2a2 and R2c2; for the three hydrogens in the $-CH_3$ position, two of them are equivalent, and the third is different from them, denoted by channels R2b2-α and R2b2-β, respectively. All channels involved in the reaction of SC_2 with OH radicals are shown as follows:

$$\begin{aligned} CH_3CH_2CH_2F\ (SC_2) + OH &\rightarrow CH_3CH_2CHF\ (P_{2a2}) + H_2O \\ &\qquad (R2a2) \\ &\rightarrow CH_2CH_2CH_2F\ (P_{2b2}) + H_2O \\ &\qquad (R2b2\text{-}\alpha,\ R2b2\text{-}\beta) \\ &\rightarrow CH_3CHCH_2F\ (P_{2c2}) + H_2O \\ &\qquad (R2c2) \end{aligned}$$

Here, a dual-level (X//Y) direct dynamics method[12−14] is applied to study the kinetic nature of the above reactions. As usual, X//Y refers to optimizations and frequencies at lower-level Y with single-point energies calculated at higher-level X. In this work, we first reported detailed electronic structure information, including the reaction path information, thermochemical quantities, barrier heights, and transition state properties for each channel. Second, the kinetic calculations are carried out on the basis of the above information by using the Polyrate 9.3 program.[15] The rate constants are calculated by the variational transition state theory (VTST).[16−18] The theoretical and experimental results are compared. Furthermore, the temperature dependence of the rate constant and the branching ratios are discussed.

In addition, it is known that the knowledge of the enthalpy of formation of the species is important in the thermodynamic properties as well as in the kinetics of atmospheric processes. However, the reactants and products radicals involved in these reactions have been little studied experimentally. In the present work, the enthalpies of formation of these species are estimated theoretically by using the isodesmic reactions.[19]

Calculation Methods

The electronic structure calculations are carried out by the Gaussian 03 program.[20] The geometries and frequencies of all the stationary points including reactants, transition states (TSs), products, and complexes are optimized by Becke's three-parameter nonlocal-exchange gradient-corrected functional[21] with the nonlocal correlational of Lee, Yang, and Parr[22] (B3LYP) method with the 6-311G(d,p) basis set. The minimum energy path (MEP) is obtained by the intrinsic reaction coordinate (IRC) theory to confirm that the TS really connects to minima along the reaction path. To obtain more reliable energy information, single-point energy calculations for the stationary points and a few extra points along the MEP are carried out at the MC-QCISD/3 (multicoefficient correlation method based on quadratic configuration interaction with single and double excitations version 3)[23] level using the B3LYP geometries. The energy profiles are further refined with interpolated single-point energies (ISPE) method,[24] where 6 points (ISPE-6) are used for spline interpolation. And the interpolation is based on the reactant well and product well.

By means of the POLYRATE-Version 9.3 program, the theoretical rate constant for each reaction channel is calculated using the conventional transition state theory (TST) and canonical variational transition state theory (CVT),[25−27] and the tunneling correction is considered by the centrifugal-dominant small-curvature semiclassical adiabatic ground-state (CD-SC-SAG)[28] method, which is computed with equal segments in the Boltzmann and θ integrals, and the number of Gauss−Legendre quadrature points is chosen as 40 for computing the Boltzmann average. Also, the sixth-order Lagrangian interpolation is used to obtain the values of the effective mass for the CD-SCSAG tunneling calculation. The lowest-frequency vibrational mode of the generalized transition state is treated as the hindered rotor,[29,30] and all of the other modes are treated by the quantum-mechanical separable harmonic oscillator approximation. For a hindered rotor, we use the RW scheme, where R stands for applying the rectilinear model for calculating the reduced moment of inertia (I_j) of the rotator and the W means using the rotational barrier height (W) from direct ab initio calculation to estimate the vibrational frequency (ω_j). The vibrational frequency can be estimated by

$$\omega_j = (W_j/2I_j)^{1/2}M \tag{1}$$

where M is the total number of minima along the torsional coordinate in the range $0-2\pi$. Here, the value of W_j is 1000 cm^{-1} and the values of M are 2 for reaction R1 and 3 for reaction R2, respectively. During the kinetic calculations, the Euler single-step integrator with a step size of 0.001 $(amu)^{1/2}$ is used to follow the MEP, and the generalized normal-mode analysis is performed every 0.01 $(amu)^{1/2}$ bohr. In the calculation of the electronic partition functions, the two electronic states for OH radicals, with a 140 cm^{-1} splitting in the $^2\Pi$ ground state, are included. The curvature components are calculated using a quadratic fit to obtain the derivative of the gradient with respect to the reaction coordinate. The total rate constants are obtained from the sum of the individual rate constants.

It is well-known that the isodesmic reaction is a relatively inexpensive and accurate method to predict the enthalpy of formation, because the conservation of the number of electron pairs in the reactants and products and the similarity of bond type cancel the systematic errors in the calculations. Here, we predict the enthalpies of the formation of the reactants CH_3CHFCH_3 and $CH_3CH_2CH_2F$ (SC_1 or SC_2) and product radicals CH_3CFCH_3, CH_3CHFCH_2, CH_3CH_2CHF, $CH_2CH_2CH_2F$, and CH_3CHCH_2F using the following isodesmic reactions,

$$CH_3CHFCH_3 + CH_4 \rightarrow CH_3F + CH_3CH_2CH_3 \tag{R3}$$

$$CH_3CH_2CH_2F\ (SC_1 \text{ or } SC_2) + CH_4 \rightarrow CH_3F + CH_3CH_2CH_3 \tag{R4}$$

$$CH_3CFCH_3 + CH_4 \rightarrow CH_3F + CH_3CHCH_3 \tag{R5}$$

$$CH_3CHFCH_2 + CH_4 \rightarrow CH_3F + CH_3CH_2CH_2 \quad (R6)$$

$$CH_3CH_2CHF + CH_4 \rightarrow CH_3F + CH_3CH_2CH_2 \quad (R7)$$

$$CH_2CH_2CH_2F + CH_4 \rightarrow CH_3F + CH_3CH_2CH_2 \quad (R8)$$

$$CH_3CHCH_2F + CH_4 \rightarrow CH_3F + CH_3CHCH_3 \quad (R9)$$

Energies of the reactants and product radicals involved in reactions R3−R9 are calculated at the MC-QCISD/3 and BMC-CCSD (a multicoefficient correlation method based on couple cluster theory with single and double excitations (CCSD) proposed by Lynch and Truhlar)[31] levels based on B3LYP/6-311G(d,p) optimized geometries.

Results and Discussion

A. Stationary Points. The geometries of all the stationary points involved in these two reactions are optimized at the B3LYP/6-311G(d,p) level. Owing to the similarity, Figure 1 only shows the optimized structures of the reactants and transition states involved in reaction channels R1a, R1b-γ, and R2a (including channels R2a1-β and R2a2), R2b (including channels R2b1-γ and R2b2-α), and R2c (including channels R2c1-β and R2c2) as the representatives of H-abstraction from each group. And the geometric parameters of other stationary points (including product radicals, other transition states and the complexes) are displayed in Supporting Information (Figure S1). From Figure 1 we can see that the reactant CH_3CHFCH_3 possesses C_1 symmetry instead of C_s symmetry considering the effect of the steric hindrance. With respect to the transition states TS_{1a} and $TS_{1b-\gamma}$, the breaking C−H bond is stretched by 3.8% and 12.1% compared to the C−H equilibrium bond length of CH_3CHFCH_3 and the forming bond H−O is longer than the equilibrium bond length in H_2O by 63.3% and 35.9%, respectively. Two stable conformers of $CH_3CH_2CH_2F$, SC_1, and SC_2, are found. SC_1, F11 lies behind H6 and H7 with C_1 symmetry, and SC_2, F11 lies between H6 and H7 with C_s symmetry, as shown in Figure 1. For the reaction SC_1 with OH radical, seven TSs are located according to the different positions of seven hydrogens, and they are designated $TS_{2a1-\alpha}$, $TS_{2a1-\beta}$, $TS_{2b1-\alpha}$, $TS_{2b1-\beta}$, $TS_{2b1-\gamma}$, $TS_{2c1-\alpha}$, and $TS_{2c1-\beta}$. However, for SC_2 with C_s symmetry, four TSs are found and they are labeled TS_{2a2}, $TS_{2b2-\alpha}$, $TS_{2b2-\beta}$, and TS_{2c2}. Similarly, Figure 1 only shows the optimized key structural parameters of $TS_{2a1-\beta}$, $TS_{2b1-\gamma}$, $TS_{2c1-\beta}$, and TS_{2a2}, $TS_{2b2-\alpha}$, and TS_{2c2}. It is easy to see that the geometries of transition states involved in hydrogen-abstraction from the same groups of SC_1 and SC_2 are similar. For example, in the transition states $TS_{2a1-\beta}$ and TS_{2a2},

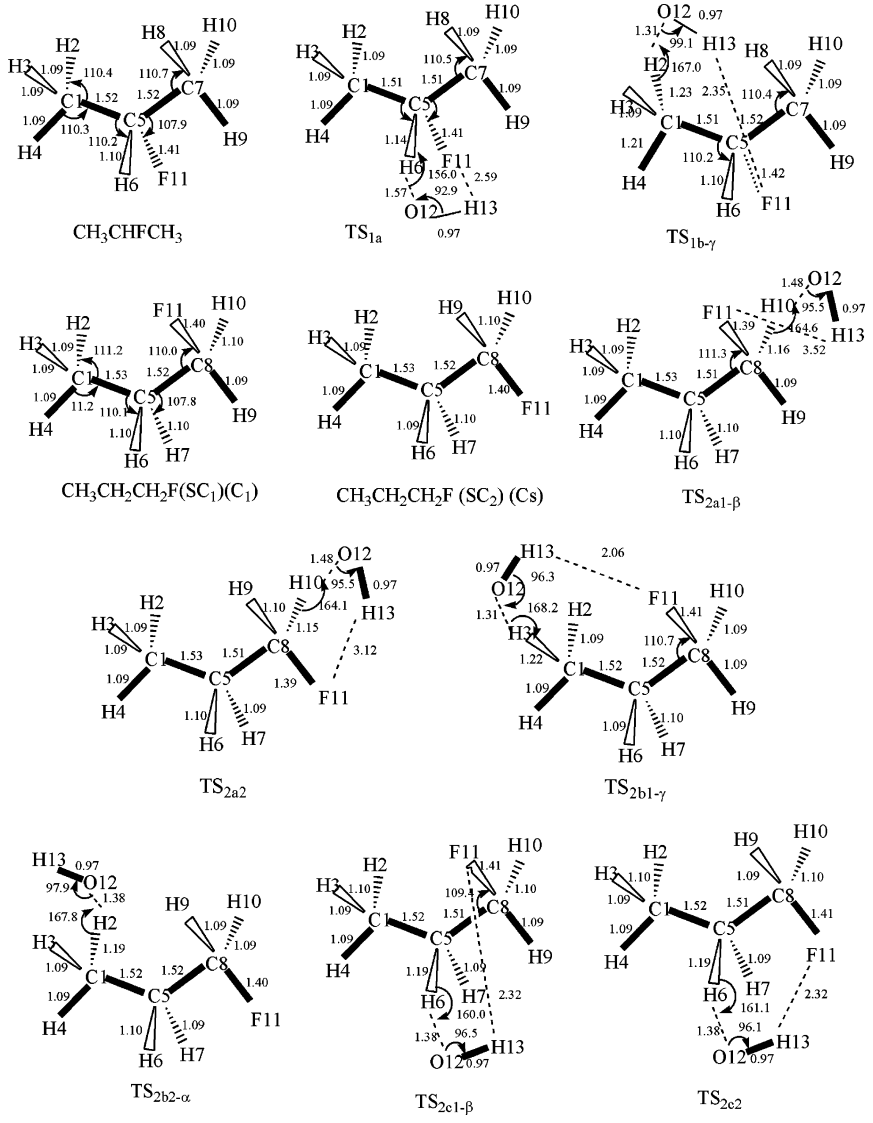

Figure 1. Optimized geometries parameters (in Å and degree) of the reactants and primary transition states (TSs) at the B3LYP/6-311G(d,p) level.

TABLE 1: Enthaplies of Reactions (ΔH_{298}° in kcal/mol) Calculated at the MC-QCISD/3//B3LYP/6-311G(d,p) Level

reactions	MC-QCISC-3//B3LYP
$CH_3CHFCH_3 + OH \rightarrow CH_3CFCH_3 + H_2O$	−21.81
$\rightarrow P_{1a-\alpha} + H_2O$	−16.63
$\rightarrow P_{1a-\beta} + H_2O$	−16.65
$\rightarrow P_{1a-\gamma} + H_2O$	−16.83
$CH_3CH_2CH_2F(SC_1) + OH \rightarrow P_{2a1-\alpha} + H_2O$	−20.20
$\rightarrow P_{2a1-\beta} + H_2O$	−20.39
$\rightarrow P_{2b1} + H_2O$	−18.26
$\rightarrow P_{2c1-\alpha} + H_2O$	−20.24
$\rightarrow P_{2c1-\beta} + H_2O$	−19.95
$CH_3CH_2CH_2F(SC_2) + OH \rightarrow P_{2a2} + H_2O$	−20.60
$\rightarrow P_{2b2} + H_2O$	−18.36
$\rightarrow P_{2c2} + H_2O$	−19.79

corresponding to H-abstraction from the $-CH_2F$ group in SC_1 and SC_2, the reactive bond C−H, which is broken, is elongated by about 5.8% and 4.5% compared to the equilibrium bond length of the isolated reactants, and the forming bond H−O is longer than the equilibrium bond length of H_2O by 54.3% and 59.4%, respectively. For these transition states, the elongation of the breaking bond (C−H) is much less than the elongation of the forming bond (H−O), indicating that the transition states are reactant-like, so these reactions may proceed via "early" transition states. When hydrogen atom is abstracted from the $-CH_3$ or $-CH_2-$ position in $CH_3CH_2CH_2F$, i.e., channels 2b and 2c, the corresponding transition states have similar "early" character, as shown in Figure 1 and Figure S1, as expected for exothermic reactions. Also, due to the high electronegativity of the fluorine atom, hydrogen bonds are formed in the transition states TS_{1a} and $TS_{1b-\gamma}$, with F11−H13 bond distances of 2.59 and 2.35 Å. The analogous six-membered ring structure in $TS_{1b-\gamma}$ makes it have a lower energy and more steady than $TS_{1b-\alpha}$ and $TS_{1b-\beta}$. In addition, owing to the high electronegativity of the oxygen atom or fluorine atom, hydrogen-bonded complexes are formed at the entrance or exit channels of reactions R1 and R2. The optimized geometries are shown in Figure S1.

The harmonic vibrational frequencies of all the stationary points are calculated at the B3LYP/6-311G(d,p) level to confirm the stationary nature and to make zero-point energy (ZPE), as well as thermal corrections. The number of imaginary frequencies (0 or 1) indicates whether a minimum or a transition state has been located. All of the minima including reactants, products, and complexes correspond to all real frequencies, but the transition states are confirmed to have one and only one imaginary frequency. In the Supporting Information, Table S1a−c displays the calculated harmonic vibrational frequencies of all the stationary points, as well as the available experimental values of OH and H_2O.

The reaction enthalpies (ΔH_{298}°) at 298 K for the two reactions at the MC-QCISD/3//B3LYP level are listed in Table 1. It is shown that all the individual reactions are exothermic reactions and the calculated enthalpies of reactions (ΔH_{298}° in kcal/mol) are decreased by about 3−5 kcal/mol when the higher MC-QCISD/3//B3LYP method is used. Table 1 also shows that the values of ΔH_{298}° for reaction channels involved in H-abstraction from the same group are very closed; for example, the values of ΔH_{298}° for channels R1b-α, R1b-β, and R1b-γ are −16.33, −16.65, and −16.83 kcal/mol. Thus, it is reasonable to choose the lowest-energy radicals as representative for estimating the enthalpies of formation and the bond energies.

Except for reactant CH_3CHFCH_3, there are no available experimental enthalpies of formation ($\Delta H_{f,298}$°) for other species involved in the title reactions. Thus, in the present study, their $\Delta H_{f,298}$° values are estimated by using isodesmic reactions R3−R9. The geometrical parameters and harmonic vibrational frequencies of all species involved in reactions R3−R9 are calculated at the B3LYP/6-311G(d,p) level, and the single point energies are calculated at the MC-QCISD/3 level. Because the energies of products $P_{1a-\alpha}$, $P_{1a-\beta}$, and $P_{1a-\gamma}$ are very close, here we select $P_{1a-\gamma}$, which possesses the lowest energies among them, to calculate the enthalpies of the formation of CH_3CHFCH_2. Similarly, the energies of product radicals $P_{2a1-\beta}$, P_{2b1}, and $P_{2c1-\alpha}$ are chosen to estimate the enthalpies of the formation of CH_3CH_2CHF, $CH_2CH_2CH_2F$, and CH_3CHCH_2F, respectively. Then, the calculated reaction enthalpies of reactions R3−R9 are combined with the known standard enthalpies of formation[32] (CH_3F, −56.03 kcal/mol; CH_4, −17.90 kcal/mol; $CH_3CH_2CH_3$, −25.04 ± 0.12 kcal/mol; CH_3CHCH_3, 21.52 ± 0.48 kcal/mol; $CH_3CH_2CH_2$, 23.91 ± 0.48 kcal/mol) to estimate the $\Delta H_{f,298}$° values of these species. To testify the reliability, the BMC-CCSD method is also used to refine the energies based on B3LYP geometries. The calculated results at two higher levels are listed in Table 2, along with the experimental values.[33−36] It is seen that the estimated enthalpies of formation of all the species at the MC-QCISD/3//B3LYP level are very close to the results obtained at the BMC-CCSD//B3LYP level, and both of them are in good agreement with the experimental ones, with the error 1.4%−2.4%. Because of the good agreement between theoretical and experimental values, it is reasonable to believe that the present predicted $\Delta H_{f,298}$°values for these species are reliable.

Schematic potential energy profiles of each reaction with zero-point energy (ZPE) corrections are plotted in Figure 2a, 2b-1, and 2b-2. From Figure 2a, we can see that the barrier height of reaction channel R1a is lower by about 1.6−3.3 kcal/mol than the ones of reaction channel R1b (including channels R1b-α, R1b-β, and R1b-γ) and channel R1a is more exothermic by about 5 kcal/mol than channel R1b. Thus, we infer that for

TABLE 2: Enthalpies of Formation (in kcal/mol) for the Reactants CH_3CHFCH_3, $CH_3CH_2CH_2F$, and Product Radicals CH_3CFCH_3, CH_3CHFCH_2, CH_3CH_2CHF, $CH_2CH_2CH_2F$, and CH_3CHCH_2F at the B3LYP/6-311G(d,p), MC-QCISD/3//B3LYP/6-311G(d,p), and BMC-CCCSD//B3LYP/6-311G(d,p) Levels

species	B3LYP	MC-QCISD/3	BMC−CCCSD	exptl
CH_3CHFCH_3	−75.21 ± 0.12	−74.38 ± 0.12	−74.52 ± 0.12	−75.4 ± 0.5[a] −76.2 ± 1.0[b] −75.5[c] −75.4[d]
$CH_3CH_2CH_2F(SC_1)$	−70.56 ± 0.12	−69.47 ± 0.12	−69.40 ± 0.12	
$CH_3CH_2CH_2F(SC_2)$	−70.11 ± 0.12	−69.19 ± 0.12	−69.37 ± 0.12	
CH_3CFCH_3,	−29.90 ± 0.48	−28.21 ± 0.48	−28.39 ± 0.48	
$CH_3CHFCH_2(P_{1a-\gamma})$	−24.64 ± 0.48	−23.63 ± 0.48	−23.73 ± 0.48	
CH_3CH_2CHF ($P_{2a1-\beta}$)	−24.44 ± 0.48	−22.27 ± 0.48	−22.53 ± 0.48	
$CH_2CH_2CH_2F$ (P_{2b1})	−21.63 ± 0.48	−20.69 ± 0.48	−20.87 ± 0.48	
CH_3CHCH_2F ($P_{2c1-\alpha}$)	−22.62 ± 0.48	−21.73 ± 0.48	−21.68 ± 0.48	

[a] From ref 33. [b] From ref 34. [c] From ref 35. [d] From ref 36.

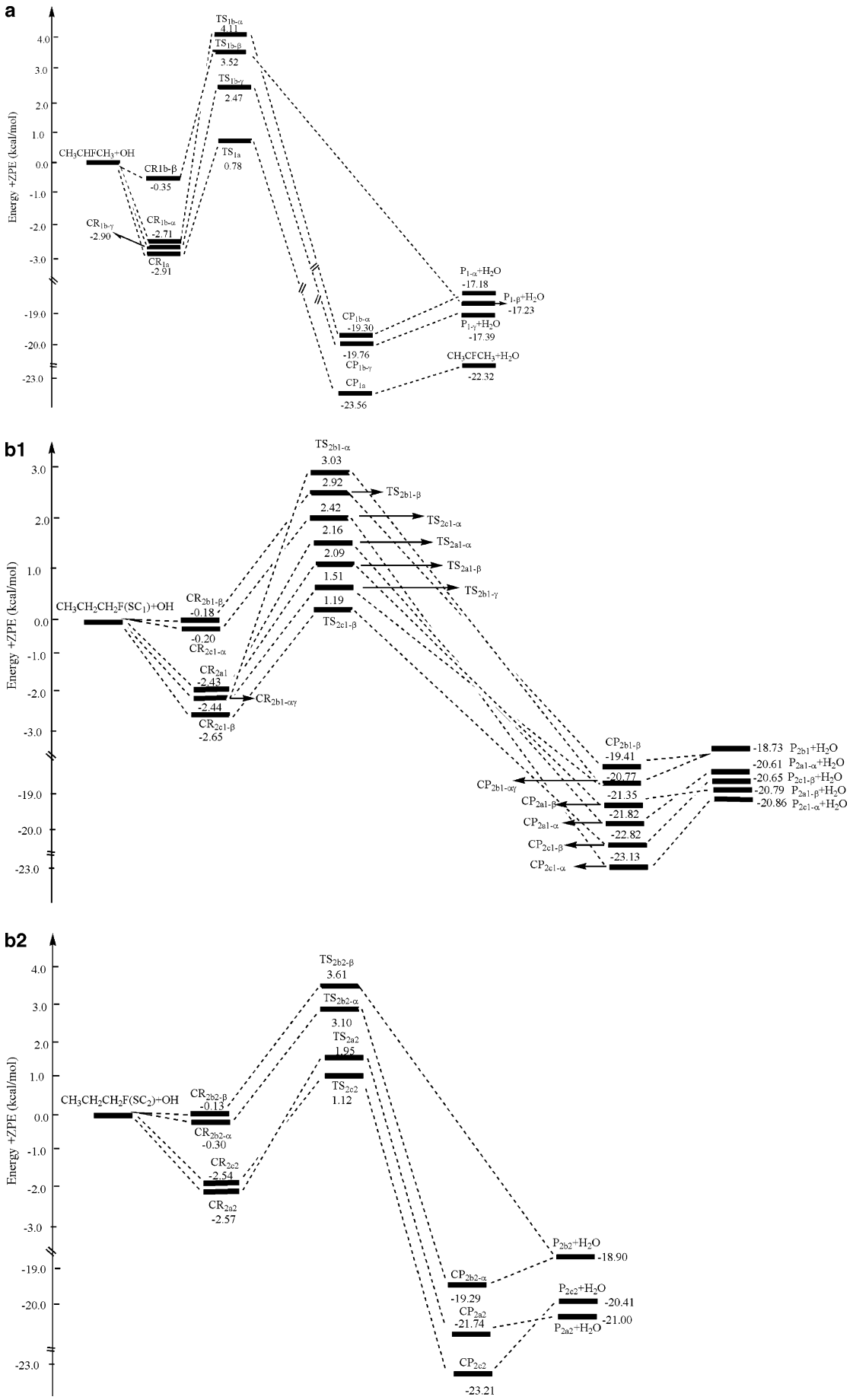

Figure 2. Schematic pathways for the reactions: (a) CH_3CHFCH_3 + OH → products; (b1) $CH_3CH_2CH_2F$ (SC_1) + OH → products; (b2) $CH_3CH_2CH_2F$ (SC_2) + OH → products. Relative energies with ZPE at the MC-QCISD-3//B3LYP/6-311G(d,p) level are in kcal/mol.

TABLE 3: C−H Bond Strengths (in kcal/mol) Calculated at the B3LYP/6-311G(d,p), MC-QCISD/3//B3LYP/6-311G(d,p), and BMC-CCSD//B3LYP/6-311G(d,p) Levels

bond	B3LYP	MC-QCISD/3	BMC-CCSD
CH_3CHCH_3-H	95.33	99.64	99.40
$CH_2CH_2CH_3-H$	99.34	102.42	102.12
CH_3CFCH_3-H	94.09	99.24	98.96
CH_2CHFCH_3-H	101.26	104.40	104.32
CH_3CH_2CHF-H	96.51	100.67	100.04
CH_3CHCH_2F-H	96.71	100.81	100.56
$CH_2CH_2CH_2F-H(SC_1)$	99.71	102.79	102.24

reaction R1, channel R1a (H-abstraction from −CHF− position) is kinetic and thermodynamically more favorable than channel R1b (H-abstraction from the $-CH_3-$ position). Also, the barrier heights of channels R1b-α, R1b-β, and R1b-γ decrease in the order $\Delta E_{1b-\alpha}$ (4.11 kcal/mol) > $\Delta E_{1b-\beta}$ (3.52 kcal/mol) > $\Delta E_{1b-\gamma}$ (2.47 kcal/mol). By analysis, we find that for channel R1b-α, the abstracted hydrogen (H4) lies between H6 and F11, whereas for channels R1b-β and R1b-γ, the abstracted hydrogen (H2 and H3) lies behind H6 and F11, so the steric hindrance for channel R1b-α is a little larger than the ones for channels R1b-β and R1b-γ; thus, channel R1b-α has the highest potential energy barrier. By comparing channels R1b-β and R1b-γ, though both of the abstracted hydrogen atoms (H3 and H2) lie behind the H6 and F11, the six-membered ring structure of transition state $TS_{1b-\gamma}$ leads to the decrease of barrier height. Similarly, for reaction $CH_3CH_2CH_2F$ with OH radicals, due to the effect of the analogous ring structure or steric hindrance, the barrier heights involved in the H-abstraction reaction channels from the same groups are slightly different. For example, the correspondingly barriers with ZPE corrections for reaction channels R2a1-α, R2a1-β, and R2a2, which are involved in the H-abstraction from the $-CH_2F$ group, are 2.16, 2.09, and 1.95 kcal/mol, respectively, at the MC-QCISD/3//B3LYP level, as shown in Figure 2b-1,b-2. Comparing the barriers and reaction enthalpies of reaction channels R2c (R2c1 or R2c2) with channels R2b (R2b1 or R2b2) and R2a (R2a1 or R2a2), we can find that channel R2c possesses the lowest barrier and is more exothermic, which indicates channel R2c is the major reaction channel for R2. If we use the formula $E_{a,298} = \Delta E^* + nRT = V^* + \Delta ZPE + \Delta E(T) + nRT$ as a simple estimation of the activation energy,[36] where V^*, ΔZPE, R, T, and $\Delta E(T)$ represent the potential barrier height, zero point energy correction, gas constant, temperature, and thermal energy correction, the estimated activation energies of the major reaction channels (R1a, R2c1-β, and R2c2) for reactions R1 and R2 are 0.72, 0.88, and 0.79 kcal/mol, respectively. Our result (0.72 kcal/mol for R1a) is much closer to the experimental value of 0.99 kcal/mol, which indicates that the estimated activation energies of the other reaction channels are reliable and the MC-QCISD/3 method is a good choice to refine the energies of these systems.

The reactivity based on the barrier heights is in line with the C−H bond energies (D_{298}). The calculated D_{298}°at the MC-QCISD/3//B3LYP and BMC-CCSD//B3LYP levels are given in Table 3. It can be seen that the results obtained at the MC-QCISD/3//B3LYP and BMC-CCSD//B3LYP levels are in good agreement, with the largest deviation being about 0.6 kcal/mol. For CH_3CHFCH_3, the bond energies increase in the order D_{298}°(−CHF−) < D_{298}°($-CH_3$), and the latter is larger than the former by about 5 kcal/mol at the MC-QCISD/3//B3LYP level, which indicates that reaction R1 would proceed mainly via the H-abstraction from the fluorinated methylene (−CHF−) position. However, for $CH_3CH_2CH_2F$ (including two rotamers SC_1 and SC_2), we can see that at the MC-QCISD/3//B3LYP level, the bond energies D_{298}°($-CH_2F-$) are almost equal to D_{298}°($-CH_2-$) and both of them are about 3 kcal/mol lower than D_{298}°($-CH_3-$). This result suggests that for reaction R2, channels R2a and R2c are more favorable than channel R2b. Furthermore, to discuss the effect of the position of F atom on the reactivity of the H atoms, we calculated the C−H bond energies of $CH_3CH_2CH_3$, which is the parent of CH_3CHFCH_3 and $CH_3CH_2CH_2F$; the corresponding results are also listed in the same table. When the C−H bond energies are compared among $CH_3CH_2CH_3$, CH_3CHFCH_3, and $CH_3CH_2CH_2F$, it is easily seen that fluorine substitution increases the reactivity of the H linking with fluorine-substituted carbon and decreases the reactivity of other H atoms.

B. Rate Constants Calculation. Dual-level dynamics calculations of two hydrogen abstraction reactions R1 and R2 are carried out with the VTST-ISPE approach. The rate constants of each reaction channel are evaluated by the conventional transition state theory (TST) and canonical variation transition state theory (CVT) over a wide temperature region from 200 to

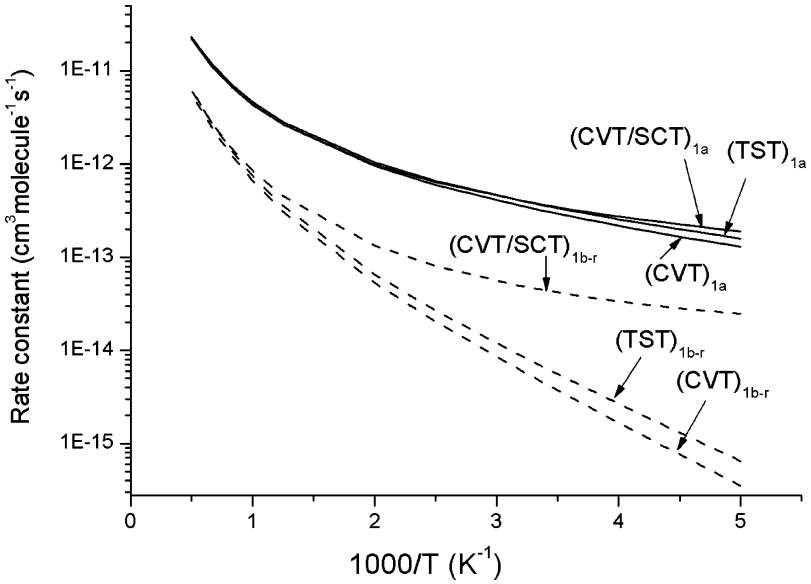

Figure 3. Plots of the TST, CVT, and CVT/SCT rate constants calculated at the MC-QCISD//B3LYP/6-311G(d,p) level vs 1000/T between 200 and 2000 K for $CH_3CHFCH_3 + OH \rightarrow CH_3CFCH_3 + H_2O$ (R1a).

TABLE 4: Calculated CVT/SCT Rate Constants (in cm^3 molecule^{-1} s^{-1}) in the Temperature Range 200−2000 K at the MC-QCISD/3//B3LYP/6-311G(d,p) Level of Theory

(a) For the Reaction $CH_3CHFCH_3 + OH \rightarrow$ Products

T (K)	k_{1a}	$k_{1b-\alpha}$	$k_{1b-\beta}$	$k_{1b-\gamma}$	k_{1b}	k_1	expl
200	2.27×10^{-13}	2.34×10^{-16}	6.68×10^{-16}	2.47×10^{-14}	2.56×10^{-14}	2.52×10^{-13}	
225	2.75×10^{-13}	6.83×10^{-16}	1.56×10^{-15}	2.88×10^{-14}	3.10×10^{-14}	3.06×10^{-13}	
250	3.28×10^{-13}	1.69×10^{-15}	3.21×10^{-15}	3.36×10^{-14}	3.85×10^{-14}	3.67×10^{-13}	
251	3.31×10^{-13}	1.75×10^{-16}	3.30×10^{-15}	3.38×10^{-14}	3.89×10^{-14}	3.70×10^{-13}	
275	3.87×10^{-13}	3.67×10^{-15}	5.99×10^{-15}	3.92×10^{-14}	4.89×10^{-14}	4.36×10^{-13}	
288	4.20×10^{-13}	5.27×10^{-15}	8.01×10^{-15}	4.24×10^{-14}	5.57×10^{-14}	4.76×10^{-13}	5.33×10^{-13}[a]
298	4.46×10^{-13}	6.84×10^{-15}	9.90×10^{-15}	4.51×10^{-14}	6.18×10^{-14}	5.08×10^{-13}	4.3×10^{-13}[a] 5.7×10^{-13}[a]
300	4.51×10^{-13}	7.19×10^{-15}	1.03×10^{-14}	4.56×10^{-14}	6.31×10^{-14}	5.14×10^{-13}	5.71×10^{-13}[a]
314	4.89×10^{-13}	1.01×10^{-14}	1.36×10^{-14}	4.96×10^{-14}	7.33×10^{-14}	5.62×10^{-13}	
325	5.21×10^{-13}	1.30×10^{-14}	1.67×10^{-14}	5.29×10^{-14}	8.26×10^{-14}	6.04×10^{-13}	6.5×10^{-13}[a]
350	5.96×10^{-13}	2.19×10^{-14}	2.55×10^{-14}	6.11×10^{-14}	1.09×10^{-13}	7.05×10^{-13}	7.26×10^{-13}[a]
375	6.77×10^{-13}	3.49×10^{-14}	3.74×10^{-14}	7.03×10^{-14}	1.43×10^{-13}	8.19×10^{-13}	7.99×10^{-13}[a]
394	7.43×10^{-13}	4.83×10^{-14}	4.87×10^{-14}	7.80×10^{-14}	1.75×10^{-13}	9.18×10^{-13}	8.52×10^{-13}[a]
400	8.59×10^{-13}	5.33×10^{-14}	7.20×10^{-14}	9.20×10^{-14}	2.42×10^{-13}	1.10×10^{-12}	
500	1.18×10^{-12}	2.07×10^{-13}	1.58×10^{-13}	1.34×10^{-13}	4.99×10^{-13}	1.68×10^{-12}	
800	3.15×10^{-12}	1.72×10^{-12}	1.24×10^{-12}	4.54×10^{-13}	3.41×10^{-12}	6.56×10^{-12}	
1000	5.19×10^{-12}	4.74×10^{-12}	2.97×10^{-12}	8.50×10^{-13}	8.56×10^{-12}	1.38×10^{-11}	
1200	7.90×10^{-12}	1.04×10^{-11}	5.88×10^{-12}	1.44×10^{-12}	1.77×10^{-11}	2.56×10^{-11}	
1500	1.33×10^{-11}	2.56×10^{-11}	1.31×10^{-11}	2.73×10^{-12}	4.14×10^{-11}	5.47×10^{-11}	
1800	2.05×10^{-11}	5.14×10^{-11}	2.46×10^{-11}	4.61×10^{-12}	8.06×10^{-11}	1.01×10^{-10}	
2000	2.64×10^{-11}	7.55×10^{-11}	3.49×10^{-11}	6.21×10^{-12}	1.17×10^{-10}	1.43×10^{-10}	

(b) For the Reaction $CH_3CH_2CH_2F + OH \rightarrow$ Products

T (K)	k_{2a1}	k_{2b1}	k_{2c1}	k_{2a2}	k_{2b2}	k_{2c2}	k_{2a}	k_{2b}	k_{2c}	k_2
200	7.27×10^{-14}	1.26×10^{-14}	1.34×10^{-13}	1.44×10^{-14}	1.82×10^{-15}	3.08×10^{-13}	5.20×10^{-15}	8.80×10^{-15}	1.95×10^{-13}	2.56×10^{-13}
275	1.82×10^{-13}	4.02×10^{-14}	2.54×10^{-13}	3.38×10^{-14}	1.39×10^{-14}	3.91×10^{-13}	1.24×10^{-13}	2.99×10^{-14}	3.07×10^{-13}	4.61×10^{-13}
298	2.31×10^{-13}	5.62×10^{-14}	3.10×10^{-13}	4.22×10^{-14}	2.24×10^{-14}	4.23×10^{-13}	1.56×10^{-13} *1.90×10^{-13}*[a]	4.26×10^{-14} *8.70×10^{-14}*[a]	3.55×10^{-13} *3.00×10^{-14}*[a]	5.53×10^{-13} *5.70×10^{-13}*[a]
350	3.71×10^{-13}	1.11×10^{-13}	4.68×10^{-13}	6.60×10^{-14}	5.50×10^{-14}	5.08×10^{-13}	2.44×10^{-13}	8.76×10^{-14}	4.85×10^{-13}	8.16×10^{-13}
375	4.54×10^{-13}	1.48×10^{-13}	5.67×10^{-13}	8.00×10^{-14}	7.91×10^{-14}	5.53×10^{-13}	2.97×10^{-13}	1.19×10^{-13}	5.61×10^{-13}	9.77×10^{-13}
400	5.48×10^{-13}	1.94×10^{-13}	6.81×10^{-13}	9.58×10^{-14}	1.10×10^{-13}	6.03×10^{-13}	3.56×10^{-13}	1.58×10^{-13}	6.47×10^{-13}	1.16×10^{-12}
425	6.53×10^{-13}	2.49×10^{-13}	8.10×10^{-13}	1.13×10^{-13}	1.48×10^{-13}	6.55×10^{-13}	4.21×10^{-13}	2.05×10^{-13}	7.43×10^{-13}	1.36×10^{-12}
500	1.05×10^{-13}	4.75×10^{-13}	1.29×10^{-12}	1.79×10^{-13}	3.18×10^{-13}	8.36×10^{-13}	6.64×10^{-13}	4.06×10^{-13}	1.09×10^{-12}	2.16×10^{-12}
800	4.02×10^{-12}	2.80×10^{-12}	5.03×10^{-12}	6.69×10^{-13}	2.30×10^{-12}	1.95×10^{-12}	2.47×10^{-12}	2.57×10^{-12}	3.61×10^{-12}	8.64×10^{-12}
1000	7.66×10^{-11}	6.16×10^{-12}	9.88×10^{-12}	1.26×10^{-12}	5.31×10^{-12}	3.12×10^{-12}	4.65×10^{-11}	5.76×10^{-12}	6.70×10^{-12}	1.71×10^{-11}
1200	1.29×10^{-11}	1.15×10^{-11}	1.71×10^{-11}	2.11×10^{-12}	1.03×10^{-11}	4.69×10^{-12}	7.80×10^{-11}	1.09×10^{-11}	1.12×10^{-11}	3.00×10^{-11}
1500	2.45×10^{-11}	2.35×10^{-11}	3.34×10^{-11}	3.98×10^{-12}	2.28×10^{-11}	7.94×10^{-12}	1.47×10^{-11}	2.31×10^{-11}	2.12×10^{-11}	5.90×10^{-11}
1800	4.10×10^{-11}	4.23×10^{-11}	5.69×10^{-11}	6.66×10^{-12}	4.24×10^{-11}	1.24×10^{-11}	2.44×10^{-11}	4.23×10^{-11}	3.54×10^{-11}	1.02×10^{-10}
2000	5.50×10^{-11}	5.90×10^{-11}	7.70×10^{-11}	8.96×10^{-12}	6.01×10^{-11}	1.61×10^{-11}	3.27×10^{-11}	5.95×10^{-11}	4.75×10^{-11}	1.40×10^{-11}

[a] From ref 10.

2000 K. Tunneling is included by means of the small-curvature tunneling (SCT) correction. Because reaction channels R1a and R1b-γ are the favorable channels of reactions R1a and R1b and the other H-abstraction reaction channels are similar to them, here, we choose these two reaction channels as representatives to analyze the variational and tunneling effects. Figure 3 shows the plots of TST, CVT, and CVT/SCT rate constants of the above two reaction channels as functions of the reciprocal of the temperature. From them we can find that at lower temperatures the variational effect plays an important role for each H-abstraction reaction. For example, the ratios of k(CVT)/k(TST) for channels R1a and R1b-γ are 0.77 and 0.54 at 200 K, respectively. However, with increasing temperature, the TST values are almost same as the CVT ones, implying that the variational effect is negligible at higher temperature. On the other hand, by contrasting the CVT and CVT/SCT, the SCT correction should be taken into account in the rate constant calculation for each reaction at a low-temperature range, with k(CVT/SCT)/k(CVT) ratios of 1.55 and 69.9 at 200 K for R1a and R1b-γ, respectively.

The total rate constants for reaction $CH_3CH_2FCH_3$ with OH radicals are obtained from the sum of the individual rate constants ($k_1 = k_{1a} + k_{1b} = k_{1a} + k_{1b-\alpha} + k_{1b-\beta} + k_{1b-\gamma}$). Because we assume two $-CH_3$ groups are equivalent, the symmetry factor $\sigma = 2$ for the reaction channels R1b-α, R1b-β, and R1b-γ are taken into account. The calculated CVT/SCT rate constants of each reaction channel and the total rate constants together with the corresponding experimental data are displayed in Table 4a, and the temperature dependence of the total constant for this reaction is also present in Figure 4a. It is seen that the theoretical rate constants of R1 are in good agreement both with the experimental values and the theoretical estimation by empirical rules,[11] and the deviation remains within a factor of about 0.9−1.2. The Arrhenius expressions $k_1 = 5.32 \times 10^{-12} \exp(-701.6/T)$ and $k_1 = 5.63 \times 10^{-12} \exp(-715.8/T)$ cm^3 molecule^{-1} s^{-1} fitted by the CVT/SCT rate constants in the temperature range 288−394 and 272−425 K are in good accord with the ones obtained by the experimental and empirical rules reported by DeMore et al., $k_1 = 3.06 \times 10^{-12} \exp(-503/T)$ and $k_1 = 3.6 \times 10^{-12} \exp(-632/T)$ cm^3 molecule^{-1} s^{-1}. However, in the case of $CH_3CH_2CH_2F$, the energy of SC_1 is very closed to that of SC_2, so they will both contribute to the overall reaction rate constant. The total rate constant (k_2) for this reaction can be obtained from the following expression:

$$k_2 = \omega_1 k_{sc1} + \omega_2 k_{sc2}$$
$$= \omega_1(k_{2a1} + k_{2b1} + k_{2c1}) + \omega_2(k_{2a2} + k_{2b2} + k_{2c2})$$

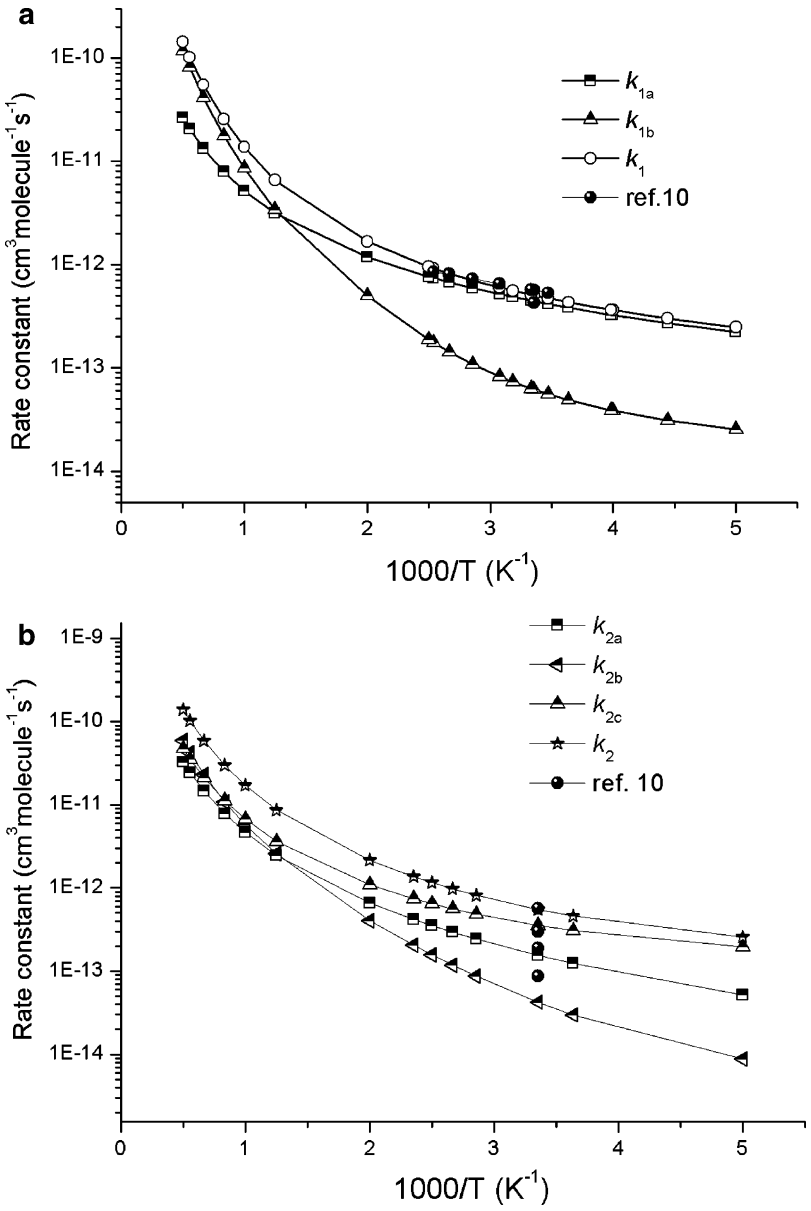

Figure 4. Total and each kind of hydrogen-abstraction reaction channel rate constants, as well as available experimental values (cm^3 molecule^{-1} s^{-1}) as functions of the reciprocal of the temperature (K) over the temperature range 200−2000 K: (a) for the reaction $CH_3CHFCH_3 + OH \rightarrow$ products; (b) for the reaction $CH_3CH_2CH_2F + OH \rightarrow$ products.

where ω_1 and ω_2 are the weight factors of each conformer calculated from the Bolzmann distribution function, k_{2a1}, k_{2a2}, k_{2b1}, k_{2b2}, k_{2c1}, and k_{2c2} are the separate rate constants of each reaction channel, and k_{sc1} and k_{sc2} are the sum rate constant for the hydrogen abstraction from the SC_1 and SC_2 isomers of CH_3-CH_2CH_2F. And because SC_2 is C_s symmetry, the symmetry factor $\sigma = 2$ for the reaction channels R2a2, R2b2-α, and R2c2 is considered in the rate constant calculation. The temperature dependence of the CVT/SCT rate constants of each channel R2a, R2b, R2c, and the total rate constant are presented in Table 4b and Figure 4b, as well as the corresponding experimental values. It can be seen that the agreement between the theoretical rate constants and the ones obtained by empirical rules is considerably good at 298 K; the factor of deviation is only 0.82 for R2a, 0.50 for R2b, 1.18 for R2c, and 0.97 for total reaction R2. The fitted expression by the CVT/SCT rate constant in 275−425 K, $k_2 = 9.42 \times 10^{-12} \exp(-840/T)$ cm^3 molecule^{-1} s^{-1}, is also in excellent agreement with $k_2 = 8.9 \times 10^{-12} \exp(-818/T)$ cm^3 molecule^{-1} s^{-1} proposed by DeMore et al.

It should be noted that for above rate constant calculations, the small curvature tunneling (SCT) correction is used, although for a reaction involving the transfer of a light particle between two heavy atoms, the large-curvature tunneling (LCT) probability may be important, especially at low temperature. It is known that the LCT correction, which is different from SCT calculation evaluated with information obtained along the MEP, can only be used where an analytic representation of the potential energy surface (PES) for a reaction is available.[37] Thus, we cannot obtain it directly from our present potential energy profile. Furthermore, to the best of our knowledge, SCT correction has been applied successfully for many similar H-abstraction reactions,[38−40] and similarly to our current study, the agreement between the CVT/SCT and the experimental rate constants is good. To further test the validation of the SCT method, the reaction path curvatures of the two reactions were calculated. The results shows that the curvatures, which are all less than 5, are not severe; therefore, the SCT correction method for these system should be suitable.

The temperature dependence of branching ratios for the two reactions is plotted in Figure 5a,b. For the reaction CH_3CHFCH_3 + OH (R1), as shown in Figure 5a, it can be found that, below 700 K, the contribution of channel R1a plays an important role in the total rate constants; for example, the values of k_{1a}/k_1 are 0.88 and 0.70 at 298 and 500 K, respectively. However, with the temperature increasing, channel R1b gradually becomes the major reaction channel. With respect to reaction $CH_3CH_2CH_2F$ + OH (R2), as shown in Figure 5b, we can see that the reaction channel R2c dominates reaction R2 below 1200 K, and reactions R2a and R2b are competitive at higher temperatures. The values of k_{2a}/k_2, k_{2b}/k_2, and k_{2c}/k_2, are 0.28, 0.08, and 0.64 at 298 K and 0.23, 0.43, and 0.34 at 2000 K, respectively.

Because there are few data available at other temperatures, for convenience of future experimental measurements, the three-parameter fits based on the CVT/SCT rate constants for the title reactions within 200−2000 K are given as follows (in cm^3 $molecule^{-1}$ s^{-1}):

$$k_{1a} = 2.05 \times 10^{-19} T^{2.44} \exp(201/T)$$

$$k_{1b} = 9.09 \times 10^{-26} T^{4.58} \exp(375.6/T)$$

$$k_1 = 3.98 \times 10^{-23} T^{3.77} \exp(528.0/T)$$

$$k_{2a} = 1.44 \times 10^{-20} T^{2.83} \exp(15.7/T)$$

$$k_{2b} = 4.68 \times 10^{-22} T^{3.39} \exp(-269.3/T)$$

$$k_{2c} = 1.44 \times 10^{-21} T^{3.16} \exp(389.2/T)$$

$$k_2 = 8.63 \times 10^{-22} T^{3.38} \exp(309.4/T)$$

Conclusions

In this paper, a dual-level direct dynamics method is employed to study the hydrogen abstraction reactions CH_3CHFCH_3 + OH and $CH_3CH_2CH_2F$ + OH. The potential energy surface information is obtained at the B3LYP/6-311G-(d,p) and MC-QCISD/3 (single-point energy) levels. For reactions CH_3CHFCH_3 + OH and $CH_3CH_2CH_2F$ + OH, each reaction proceeds via indirect mechanisms. The theoretical rate constants are calculated in the temperature range from 200 to 2000 K by canonical variational transition state theory (CVT) with a small-curvature tunneling correction (SCT) at the MC-QCISD/3//B3LYP/6-311G(d,p) level. The calculated activation energies and the CVT/SCT rate constants show good agreement with the available excremental values. For two reactions, the dominant channels are H-abstraction from the −CHF− and $-CH_2-$ groups at lower temperatures, respectively. The temperature dependence of the branching ratios is discussed. The three parameter expressions for two reactions within 200−2000 K are $k_1 = 3.98 \times 10^{-23} T^{3.77} \exp(528.0/T)$ and $k_2 = 8.63 \times 10^{-22} T^{3.38} \exp(309.4/T)$ cm^3 $molecule^{-1}$ s^{-1}. We hope the theoretical results may be useful for estimating the kinetics of the reactions over a wide temperature range where no experimental data are available. Furthermore, the enthalpies of formation of reactants CH_3CHFCH_3, $CH_3CH_2CH_2F$, and product radicals CH_3CFCH_3, CH_3CHFCH_2, CH_3CH_2CHF, $CH_2CH_2CH_2F$, and CH_3CHCH_2F are studied using isodesmic reactions at the MC-QCISD/3//B3LYP/6-311G(d,p) level.

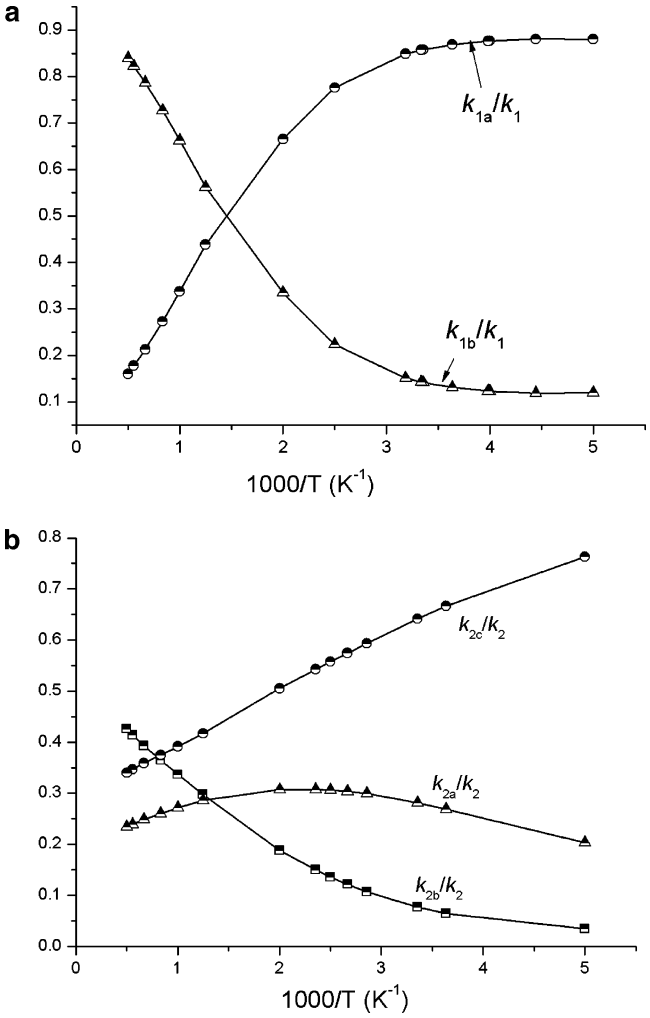

Figure 5. Calculated branching ratios vs 1000/*T* between 200 and 2000 K: (a) for the reaction CH_3CHFCH_3 + OH → products; (b) for the reaction $CH_3CH_2CH_2F$ + OH → products.

Acknowledgment. We thank Professor Donald G. Truhlar for providing the POLYRATE8.4.1 program. This work was supported by the National Natural Science Foundation of China (20303007, 20333050, and 20073014), the Doctor Foundation of the Ministry of Education, the Foundation for University Key Teacher of the Ministry of Education, the Key Subject of Science and Technology of the Ministry of Education of China, and the Key Subject of Science and Technology of the Jilin Province.

Supporting Information Available: Calculated frequencies and optimized geometries. This material is available free of charge via the Internet at http://pubs.acs.org.

References and Notes

(1) Molina, M. J.; Rowland, F. S. *Nature (London)* **1974**, *249*, 810.
(2) Hammitt, J. K.; Camm, F.; Connell, P. S.; Mooz, W. E.; Wolf, K. A.; Wuebbles, D. J.; Bamezoi, A. *Nature (London)* **1987**, *330*, 711.
(3) Rebbert, R. E.; Ausloos, P. J. *J. Photochem* **1975**, *4*, 419. Rebbert, R. E.; Ausloos, P. J. *J. Photochem* **1976/1977**, *6*, 265.
(4) Hanel, R. A. *J. Geophys. Res.* **1972**, *77*, 2629.
(5) Houghton, J. T., et al., Eds. WMO/UNEP, Climate Change 1995, The IPCC Scientific Assessment; Cambridge University Press: Cambridge, 1996.
(6) Fisher, D. A.; Hales, C. H.; Wang, W. C.; Ko, M. K. W.; Sze, N. D. *Nature (London)* **1990**, *344*, 513.
(7) WMO/UNEP, Atmospheric Ozone: 1985, World Meterological Organization Global Ozone Research and Monitoring Project-Report No. 16, World Meteorological Organization: Geneva, Switzerland, 1986.

(8) Scientific Assessment of Stratospheric Ozone: 1989, World Meteorological Organization Global Ozone Research and Monitoring Project, Report No. 20, Vol. 2 Appendix AFEAS Report, World Meteorological Organization: Geneva, Switzerland, 1990.

(9) Ravishankara, A. R.; Turnipseed, A. A.; Jensen, N. R.; Barone, S.; Mills, M. C.; Howard, J.; Solomon, S. *Science* **1994**, *263*, 71.

(10) DeMore, W. B.; Wilson, E. W., Jr. *J. Phys. Chem. A* **1999**, *103*, 573.

(11) DeMore, W. B. *J. Phys. Chem.* **1996**, *100*, 5813.

(12) Truhlar, D. G. Direct Dynamics Method for the Calculation of Reaction Rates: The Reaction Path. In *The Reaction Path in chemistry: current Approaches and Perspectives*; Heidrich, Ed.; D. Kluwer: Dordrecht, The Netherlands, 1995; p 229.

(13) Truhlar, D. G.; Garrett, B. C.; Klippenstein, S. J. *J. Phys. Chem.* **1996**, *100*, 12771.

(14) Hu, W. P.; Truhlar, D. G. *J. Am. Chem. Soc.* **1996**, *118*, 860.

(15) Corchado, J. C.; Chuang, Y.-Y.; Fast, P. L.; Hu, W.-P.; Liu Y.-P.; Lynch, G. C.; Nguyen, K. A.; Jackels, C. F.; Ramos, A. F.; Ellingson, B. A.; Lynch, B. J.; Melissas, V. S.; Villà, J.; Rossi, I.; Coitino, E. L.; Pu J.; Albu, T. V. POLYRATE, version 9.3.1; University of Minnesota: Minneapolis, 2005.

(16) Truhlar, D. G.; Garrett, B. C. *Acc. Chem. Res.* **1980**, *13*, 440.

(17) Truhlar, D. G.; Isaacson, A. D.; Garrent, B. C. *The Theory of Chemical Reaction Dynamics*; Baer, M., Ed.; CRC Press: Boca Raton, FL, 1985; p 65.

(18) Truhlar, D. G.; Garrett, B. C. *Annu. Rev. Phys. Chem.* **1984**, *35*, 159.

(19) IUPAC, http://www.iupac.org/reports/**1999**/7110minkin/i.html.

(20) Frisch, M. J.; Truck, G. W.; Schlegel, H. B.; Scuseria, G. E.; Robb, M. A.; Cheeseman, J. R.; Zakrzewski, V. G.; Montgomery, J. A., Jr.; Stratmann, R. E.; Burant, J. C.; Dapprich, S.; Millam, J. M.; Daniels, A. D.; Kudin, K. N.; Strain, M. C.; Farkas, O.; Tomasi, J.; Barone, V.; Cossi, M.; Cammi, R.; Mennucci, B.; Pomelli, C.; Adamo, C.; Clifford, S.; Ochterski, J.; Petersson, G. A.; Ayala, P. Y.; Cui, Q.; Morokuma, K.; Malick, D. K.; Rabuck, A. D.; Raghavachari, K.; Foresman, J. B.; Cioslowski, J.; Ortiz, J. V.; Boboul, A. G.; Stefnov, B. B.; Liu, G.; Liaschenko, A.; Piskorz, P.; Komaromi, L.; Gomperts, R.; Martin, R. L.; Fox, D. J.; Keith, T.; Al-Laham, M. A.; Peng, C. Y.; Nanayakkara, A.; Gonzalez, C.; Challacombe, M.; Gill, P. M. W.; Johnson, B.; Chen, W.; Wong, M. W.; Andres, J. L.; Gonzalez, C.; Head-Gordon, M.; Replogle E. S.; Pople, J. A. *GAUSSIAN 03*, revision A.1; Guassian, Inc.: Pittsburgh, PA, 2003.

(21) Becker, A. D. *J. Chem. Phys.* **1993**, *98*, 1372.

(22) Lee, C.; Yang, W.; Parr, R. G. *Phys. Rev. B* **1988**, *37*, 785.

(23) Lynch, B. G.; Truhlar, D. G. *J. Phys. Chem. A* **2003**, *107*, 3898.

(24) Chuang, Y .Y.; Corchado, J. C.; Truhlar, D. G. *J. Phys. Chem. A* **1999**, *103*, 1140.

(25) Garrett, B. C.; Truhlar, D. G. *J. Chem. Phys.* **1979**, *70*, 1593.

(26) Garrett, B. C.; Truhlar, D. G. *J. Am. Chem. Soc.* **1979**, *101*, 4534.

(27) Garrett, B. C.; Truhlar, D. G.; Grev, R. S.; Magnuson, A. W. *J. Phys. Chem.* **1980**, *84*, 1730. Erratum. *J. Phys. Chem.* **1983**, *87*, 4534.

(28) Liu, Y. P.; Lynch, G. C.; Truong, T. N.; Lu, D. H.; Truhlar, D. G.; Garrett, B. C. *J. Am. Chem. Soc.* **1993**, *115*, 2408.

(29) Truhlar, D. G. *J. Comput. Chem.* **1991**, *12*, 266.

(30) Chuang, Y. Y.; Truhlar, D. G. *J. Chem. Phys.* **2000**, *112*, 1221.

(31) Lynch, B. J.; Yan, Z.; Truhlar, D. G. *J. Phys. Chem. A* **2005**, *109*, 1643.

(32) NIST Chemistry Webbook; Linstrom, P. J., Mallard, W. G., Eds.; Available from: http://webbook.Nist.Gov/chemistry.

(33) Kormos, B. L.; Liebman, J. F.; Cramer, C. J. *J. Phys. Org. Chem.* **2004**, *17*, 656.

(34) Luo, Y.-R.; Benson, S. W. *J. Phys. Chem. A* **1997**, *101*, 3042.

(35) Smith, D. W. *J. Phys. Chem. A* **1998**, *102*, 7086.

(36) Schaffer, F.; Verevkin, S. P.; Rieger, H. J.; Beckhaus, H. D.; Ruchart, C. *Liebigs Ann. Chem.* **1997**, 1333.

(37) Pacey, P. D. *J. Chem. Educ.* **1981**, *58*, 612.

(38) Taghikhani, M.; Parsafar, G. A.; Sabzyan, H. *J. Phys. Chem. A* **2005**, *109*, 8158.

(39) Galano, A.; Alvarez-ldaboy, J. R.; Ruiz-Santoyo, M. E.; Vivier-Bunge, A. *Chem. Phys. Chem.* **2004**, *5*, 1379.

(40) Wang, Y.; Liu, J.; Li, Z.; Wang, L.; Wu, J.; Sun, C. *J. Phys. Chem. A* **2006**, *110*, 5853.